THE JOURNAL OF PHYSICAL CHEMISTRY LETTERS
A JOURNAL OF THE AMERICAN CHEMICAL SOCIETY

pubs.acs.org/JPCL

Letter

Universal Machine Learning Interatomic Potentials: Surveying Solid Electrolytes

Amir Hajibabaei and Kwang S. Kim*

Cite This: *J. Phys. Chem. Lett.* 2021, 12, 8115–8120

Read Online

ACCESS | Metrics & More | Article Recommendations | Supporting Information

ABSTRACT: We apply ab initio molecular dynamics (AIMD) with on-the-fly machine learning (ML) of interatomic potentials using the sparse Gaussian process regression (SGPR) algorithm for a survey of Li diffusivity in hundreds of ternary crystals as potential electrolytes for all-solid-state batteries. We show that models generated for these crystals can be easily combined for creating more general and transferable models which can potentially be used for simulating new materials without further training. As examples, universal potentials are created for Li−P−S and Li−Sb−S systems by combining the expert models of the crystals which contained the same set of elements. We also show that combinatorial models of different ternary crystals can be directly applied for modeling composite quaternary ones (e.g., Li−Ge−P−S). This hierarchical approach paves the way for modeling large-scale complexity by a combinatorial approach.

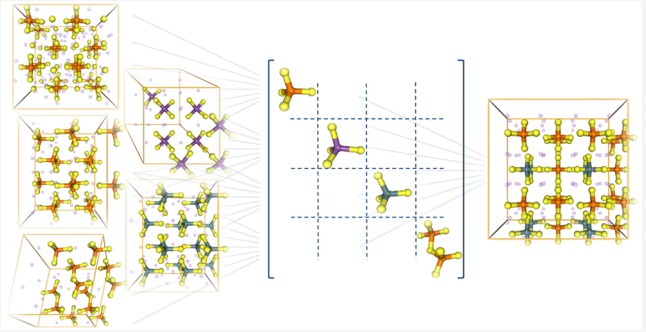

Recently, ab initio simulations such as density functional theory (DFT) have become important tools for computational studies of fast ionic diffusion in solid electrolytes (SEs)[1] for applications in safe, durable, and fast charging batteries.[2] These simulations have shed light on the diffusion mechanism of ions in SEs,[3−6] the effect of anion and cation substitutions,[7] the role of crystalline symmetry on Li conductivity,[8,9] optimal compositions,[10] SE solutions,[11] and the origin of superionic conductivity.[12]

AIMD can be used for direct simulation of the finite temperature diffusivity but it requires huge computational resources for numerous ab initio calculations. For statistical certainty, the temporal length of AIMD should be much longer than the characteristic time scale of the ionic jumps.[13] The computational cost of DFT increases as N^3 (or N^2 log N) with the number of atoms N, and so it is only practical for small systems. To overcome these limitations, great strides have been made in recent years toward ML interatomic potentials (ML-IAPs) which are trained using a set of ab initio data. Two branches are neural networks (NNs)[14−16] and kernel-based methods such as Gaussian approximation potentials (GAP),[17] gradient-domain learning,[18,19] variations of Bayesian linear regression (BLR),[20−22] and sparse Gaussian process regression (SGPR) potentials.[23] NNs are suitable for large data sets while kernel-based methods excel in training with smaller data and on-the-fly learning.[21−25] These methods have found a wide range of applications in physical chemistry.[26] Relating to SEs, Li_3N was studied using electrostatic spectral neighbor analysis potential (eSNAP) method,[27] Li_3PO_4 using NNs,[28] and $Li_7P_3S_{11}$ using SGPR.[23]

An important issue for the future of ML-IAPs is transferability and systematic model reusability. Currently, models are generated for specific tasks and often discarded afterward. The ability to build on prior models is highly desirable and imperative for efficient exploration of functional materials. Here we show that, although gradual improving of the trained models is possible with all ML methods, kernel-based methods such as SGPR offer natural frameworks for libraries of ML models that can be combined with little effort to describe increasingly complex materials. NNs memorize the data using a set of weights with fixed size and thus have to be reoptimized entirely upon adding new data. In contrast, in kernel-based methods, models are represented by a set of local chemical environments which can be easily categorized and encapsulated in libraries. We explore these ideas in the context of Li-conducting crystals, which are one of the essential components of all-solid-state storage devices. In an unsupervised fashion, hundreds of ternary crystals are simulated by on-the-fly ML molecular dynamics (MD) and 22 fastest Li conductors are distinguished. Later, we discuss combining the ML models for more transferable potentials and a combinatorial approach for modeling new crystals.

Received: May 20, 2021
Accepted: July 23, 2021
Published: August 19, 2021

https://doi.org/10.1021/acs.jpclett.1c01605
J. Phys. Chem. Lett. 2021, 12, 8115–8120

For ML-IAP, any configuration x of N atoms is compiled to a list of descriptors. A common ansatz is defining a per-atom descriptor $x = \{\rho_i\}_{i=1}^{N}$ where ρ_i depends only on the local chemical environment of atom i within a cutoff radius. Then the potential energy becomes additive over local terms

$$E(x) = \sum_{i=1}^{N} \mathcal{E}(\rho_i) \tag{1}$$

In kernel-based regression methods, $\mathcal{E}$ is expressed as

$$\mathcal{E}(\rho) = \sum_{j=1}^{m} \mathcal{K}(\rho, \chi_j) w_j = \mathbf{k}_{\rho m}\mathbf{w} \tag{2}$$

where the matrices are represented with bold fonts, $z = \{\chi_i\}_{j=1}^{m}$ is the set of reference/inducing descriptors, $\mathbf{w}$ is the vector of weights for the inducing descriptors, and $\mathcal{K}$ is a similarity/covariance kernel. The weights are obtained such that the potential energy and forces are reproduced for a set of ab initio data $X = \{x_k\}_{k=1}^{n}$ and depend on the regression algorithm. In SGPR[23]

$$\mathbf{w} = (\epsilon^2\mathbf{k}_{mm} + \mathbf{k}_{nm}^{\mathbf{T}}\mathbf{k}_{nm})^{-1}\mathbf{k}_{nm}^{\mathbf{T}}\mathbf{Y} \tag{3}$$

where $\mathbf{k}_{mm}$ and $\mathbf{k}_{nm}$ are the interinducing and data-inducing covariance matrices, $\mathbf{Y}$ represents the potential energies (and forces), and ϵ is the noise hyperparameter. The noise scale ϵ and other possible hyperparameters in the kernel $\mathcal{K}$ are optimized to maximize the likelihood of the data energies. For the similarity kernel, we use a variation of the smooth overlap of atomic positions (SOAP)[29] which we have defined in ref 23. For existing data, the inducing descriptors are sampled from the data; otherwise, with on-the-fly learning, both the data and inducing descriptors are sampled during MD.

The VASP[30] package which implements the projector augmented-wave[31] approach to DFT with PBE functionals[32] is used for all ab initio calculations (with kinetic energy cutoff of 500 eV). We used the Python package AUTOFORCE for on-the-fly generation of SGPR models.[23] For reporting the accuracy of ML potentials, we use the coefficient of determination R^2 which is defined by

$$R^2 = 1 - \frac{\sum_i (f_i - \tilde{f}_i)^2}{\sum_i (f_i - \bar{f})^2} \tag{4}$$

where $\{f_i\}$ are ab initio (DFT/PBE) forces, $\bar{f}$ is their average, and $\{\tilde{f}_i\}$ are ML forces. R^2 indicates the fraction of explained variance. Training and testing are similar to those in ref 23 and so are discussed only briefly in the Supporting Information.

In ref 23, the $Li_7P_3S_{11}$ superionic conductor is extensively studied using SGPR. We apply similar simulations to hundreds of potential SEs, focusing on ternary systems (composed of three elements) in the materialsproject[33] repository that contain Li. Crystals containing the transition metals are not considered here, which will be studied in the future. Li concentration, stability, and band gap are used as initial filters since a SE should have considerable Li atoms and it should be an electron insulator. The detailed selection criteria and a list of about 300 crystals which passed the initial filters are noted in the Supporting Information. A quaternary system of $Li_{10}GeP_2S_{12}$[34] is included in the list as an extension of the ternary system. Then *NPT*-MD simulations with on-the-fly SGPR are performed for a duration of at least ~100 ps (up to ~600 ps) for each crystal at standard pressure. Three or four temperatures are chosen for MD simulation depending on the stability against melting and the Li diffusion rate (see Supporting Information). The mean squared displacement (MSD) of atoms is defined by

$$\mathrm{MSD}(t) = \frac{1}{N}\sum_{i=1}^{N} |\Delta\vec{r}_i(t)|^2 \tag{5}$$

where N is the number of mobile ions and $\Delta\vec{r}_i(t) = \vec{r}_i(t) - \vec{r}_i(0)$. The diffusivity is defined as

$$D = \lim_{t\to\infty} \frac{1}{2dt}\langle \mathrm{MSD}(t)\rangle \tag{6}$$

where $d = 3$ is dimensions and $\langle\rangle$ indicates the ensemble average. With the assumption of an Arrhenius temperature dependence for diffusivity

$$D = D_0 e^{-E_a/k_B T} \tag{7}$$

the activation energy E_a can be calculated. The Nernst–Einstein relationship for the ionic conductivity σ is given by

$$\sigma = \frac{Nq^2}{Vk_B T} D \tag{8}$$

where N is the number of Li atoms, V is the volume, q is the ion electric charge, and T is temperature. See Figure 1 and

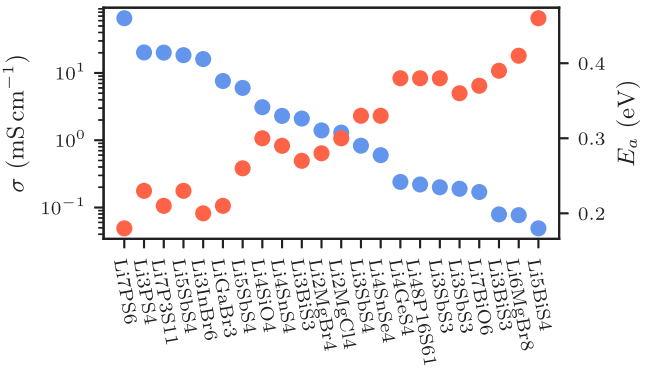

Figure 1. Extrapolated ionic conductivity at 300 K (σ in blue) and activation energy (E_a in red) for 22 fastest Li-conducting crystals.

Table 1 for Li diffusivity in the 22 fastest Li-conducting crystals. In *NPT*-MD simulations, the volume expands with increasing temperature. This temperature dependence is ignored in reporting the ionic conductivities in Table 1 since it only modifies the values by $O(1\%)$ (see ref 23). Nevertheless, the effect of the *NPT* ensemble is directly reflected in diffusivity and a significantly faster ionic conduction is observed in comparison with the *NVT* ensemble.

We should note that fast Li diffusion is one of the most important factors for a promising SE. Stability against Li metal and wide electrochemical window are other important factors which are not considered here. Additionally, experimental reports often measure long-range diffusivity which is affected by grain boundaries while the values we report in Table 1 reflect only the short-range diffusivity. Special technique is required for probing the short-range diffusivity in experimental samples.[35] Among 22 Li-conducting SEs reported in Table 1, most are sulfides[36] (14), with a few halides[37] (five), two oxides, and one selenide. Here we briefly discuss the experimental

https://doi.org/10.1021/acs.jpclett.1c01605
J. Phys. Chem. Lett. 2021, 12, 8115−8120

Table 1. The 22 Fastest Li-Conducting Ternary Solid Electrolytes Obtained after Filtering of about 300 Candidates[a]

			diffusion coefficient (Å^2/ps) at given temperature (K)									
mp-ID	formula	ML R^2	400	500	600	700	800	900	1000	1200	E_a (eV)	σ_{RT} (mS/cm)
mp-1211324	Li_7PS_6	0.972			0.15		0.29		0.54	0.83	0.18	65.2
mp-1097036	Li_3PS_4	0.972		0.068	0.14	0.28	0.46				0.23	20.2
mp-641703	$Li_7P_3S_{11}$	0.958			0.12	0.2	0.32		0.61		0.21	20.1
mp-768197	Li_5SbS_4	0.934			0.1	0.18	0.31				0.23	18.4
mp-1147621	Li_3InBr_6	0.924	0.018	0.057	0.13						0.2	16.1
mp-28327	$LiGaBr_3$	0.903		0.049	0.11						0.21	7.6
mp-756427	Li_5SbS_4	0.933				0.086	0.19	0.26	0.37		0.26	6.0
mp-685863	Li_4SiO_4	0.958					0.093	0.2	0.32	0.53	0.3	3.1
mp-1195718	Li_4SnS_4	0.973					0.18	0.32	0.37	0.74	0.29	2.3
mp-766409	Li_3BiS_3	0.946			0.034	0.077	0.12		0.29		0.27	2.1
mp-29009	Li_2MgBr_4	0.944			0.045	0.096	0.18				0.28	1.4
mp-38684	Li_2MgCl_4	0.958			0.047	0.095	0.21		0.46		0.3	1.3
mp-760415	Li_3SbS_4	0.966					0.2		0.57	0.98	0.33	0.83
mp-1194700	Li_4SnSe_4	0.962					0.15	0.3	0.41	0.8	0.33	0.6
mp-1222582	Li_4GeS_4	0.97					0.14	0.31	0.4	0.93	0.38	0.24
mp-1001069	$Li_{48}P_{16}S_{61}$	0.953			0.027	0.083	0.17				0.38	0.22
mp-1177520	Li_3SbS_3	0.929			0.018	0.058	0.18		0.39		0.38	0.2
mp-775806	Li_3SbS_3	0.944					0.084	0.16	0.27	0.49	0.36	0.19
mp-38487	Li_7BiO_6	0.987					0.041	0.079	0.12	0.25	0.37	0.17
mp-753720	Li_3BiS_3	0.939					0.08	0.14	0.21	0.51	0.39	0.079
mp-29008	Li_6MgBr_8	0.965			0.019	0.052	0.13	0.23			0.41	0.077
mp-757150	Li_5BiS_4	0.929			0.02	0.12	0.2	0.41			0.46	0.049
mp-696128	$Li_{10}GeP_2S_{12}$	0.967			0.16		0.32		0.55	0.76	0.17	84.2
mp-696138	$Li_{10}GeP_2S_{12}$	0.97			0.14		0.33		0.55	0.85	0.19	46.6

[a]Diffusivities are obtained with MLMD in the *NPT* ensemble (see Supporting Information for statistical variances). The first column is the ID of the crystal in the materialsproject[33] repository. In the last column, σ_{RT} is the extrapolated ionic conductivity at 300 K. The quaternary $Li_{10}GeP_2S_{12}$ is appended as a special case.

results for selective SEs. The top three fastest ionic conductors belong to the $Li_2S-P_2S_5$ system. The most stable compound in this system is (γ-/β-) Li_3PS_4. Li_7PS_6 is a lithium argyrodite with orthorhombic/cubic (low/high temperatures) phase where the cubic phase has a higher conductivity. The highest experimental conductivity reported in this system is for $Li_7P_3S_{11}$ which has a triclinic cell made of PS_4 tetrahedra and P_2S_7 double-tetrahedra.[38] The highest experimental room temperature ionic conductivities (mS/cm) reported so far (to the best of our knowledge) are 0.16 for Li_3PS_4,[39] 0.11 for Li_7PS_6,[40] and 17 for $Li_7P_3S_{11}$.[41] The latter is one of the highest reported to date for a SE.[36] As a halide, conductivity of ∼4 mS/cm (at 330 K) is reported for Li_3InBr_6.[42] Li_4SiO_4 has also been considered as a parent for SE solutions.[11] The experimental conductivities are often improved, even by several orders of magnitude,[39] depending on the preparation method. Our simulations suggest that experimental preparation methods can be improved, specially for Li_7PS_6.

Previously, a SGPR model is generated for each SE. We may refer to such a model as a local or expert model. An expert model i is obtained from its m_i inducing descriptors and n_i data which are sampled on-the-fly with MD. Then the covariance matrices $\mathbf{k}_{m_im_i}$ and $\mathbf{k}_{n_im_i}$ are built which yield the weights $\mathbf{w}_i$ needed for predictions (see eq 3). Each expert model can be viewed as a block from the universal SGPR model which is defined by the global covariance matrices $\mathbf{k}_{MM}$ and $\mathbf{k}_{NM}$ (with $M = \sum_i m_i$ and $N = \sum_i n_i$), where

$$\mathbf{k}_{MM} = \begin{bmatrix} \mathbf{k}_{m_1m_1} & \mathbf{k}_{m_1m_2} & \cdots \\ \mathbf{k}_{m_2m_1} & \mathbf{k}_{m_2m_2} & \cdots \\ \vdots & \vdots & \ddots \end{bmatrix} \tag{9}$$

and

$$\mathbf{k}_{NM} = \begin{bmatrix} \mathbf{k}_{n_1m_1} & \mathbf{k}_{n_1m_2} & \cdots \\ \mathbf{k}_{n_2m_1} & \mathbf{k}_{n_2m_2} & \cdots \\ \vdots & \vdots & \ddots \end{bmatrix} \tag{10}$$

where $\mathbf{k}_{m_im_j}$ and $\mathbf{k}_{n_im_j}$ (for $i \neq j$) are interexpert cross covariance matrices. Inserting these matrices into eq 3 with $\mathbf{Y} = [\mathbf{Y}_1, \mathbf{Y}_2, \ldots]^T$ results in the global weights $\mathcal{W}$. Such a model would be able to describe all SEs simultaneously and therefore would be more transferable.

But building such a universal model is computationally difficult and, even if possible, would become too slow for predictions. The assumption that the off-diagonal blocks are zero results in $\mathcal{W} = [\mathbf{w}_1, \mathbf{w}_2, \ldots]^T$ and the prediction of the universal model reduces to simple averaging over expert models. We refer to this approximation as "product of experts" (POE). POE becomes reasonable when the expert models are built for completely dissimilar materials. A better approach is to use the expert models as a library. Given a new material x which is not available in the library, we can choose only a subset of expert models which are similar to x. Algebraically, if $\mathbf{k}_{MM}$ is built from a subset of experts and

https://doi.org/10.1021/acs.jpclett.1c01605
J. Phys. Chem. Lett. 2021, 12, 8115−8120

$$\mathbf{k}_{xx} - \mathbf{k}_{xM}\mathbf{k}_{MM}^{-1}\mathbf{k}_{xM}^{\mathbf{T}} \to 0 \quad (11)$$

then the chosen subset is a sufficient model. We refer to such a combination as "fusion of experts" (FOE). If such a subset cannot be constructed, then the expert model for x should be added to the library. Since it is possible that similar inducing descriptors are repeated in several expert models, a FOE can be further compressed for increasing the efficiency. We call such a model "merging of experts" (MOE). MOE can be obtained by importance sampling of the FOE data and inducing descriptors using a threshold criterion. Here, the adaptive sampling algorithm described in ref 23 is used. In simple terms, POE is obtained by neglecting the off-diagonal blocks (cross terms) of the global covariance matrix, MOE by importance sampling of the rows/columns, and FOE by forceful inclusion of all elements.

As an example, four crystals out of 22 in Table 1 have the same set of elements (Li−P−S). The R^2 of the above combinatorial models are shown in Table 2. As expected,

Table 2. R^2 of Expert Models and Their Combinations for Li−P−S and Li−Sb−S Systems Where e, f or g, h Are Allotropes

	Li−P−S	expert	POE	MOE	FOE
a	Li_3PS_4	0.972	0.962	0.973	0.980
b	Li_7PS_6	0.972	0.813	0.966	0.978
c	$Li_{48}P_{16}S_{61}$	0.953	0.697	0.952	0.969
d	$Li_7P_3S_{11}$	0.958	0.864	0.955	0.969
	Li−Sb−S	Expert	POE	MOE	FOE
e	Li_5SbS_4	0.934	0.842	0.934	0.956
f	Li_5SbS_4	0.933	0.892	0.935	0.959
g	Li_3SbS_3	0.929	0.897	0.933	0.955
h	Li_3SbS_3	0.944	0.930	0.942	0.963
i	Li_3SbS_4	0.966	0.527	0.932	0.958

POE is worse than expert models. It is included here because in most of the non-Bayesian ML methods, averaging over the expert models is the only available mechanism for combining ML models which is equivalent to POE in Bayesian methods. The current study provides a quantitative comparison. Thus, although POE can provide a rough ML-IAP without any further ML procedures, it does not generalize well. MOE is as good as the expert models even though its size (data/inducing = 102/573) is much smaller than the combined size of the experts (181/1418). FOE has the same size as the combined size of the experts but almost in every case is even better than the experts. Thus FOE is to be preferred when affordable; otherwise, MOE offers a scalable solution. Similar combinations are shown for Li−Sb−S system in Table 2. One could accomplish the same by training a model sequentially in all domains. But the combinatorial approach above opens the door for strategies like "high level parallelism" or "a library of SGPR potentials", which can be combined by simple cross covariance calculations to describe increasingly complex materials. Such a combinatorial approach is not trivial by other methods like NNs.

As a more interesting and useful example, we combined the SGPR models for Li_3PS_4 and Li_4GeS_4 and tested it on $Li_{10}GeP_2S_{12}$ (both configurations in Table 1). Due to the presence of different species P and Ge, the combinatorial model cannot be significantly compressed, and thus, MOE and FOE are equivalent. The combined model of the two ternary crystals described the forces of the quaternary crystal with R^2 = 0.961, which is very close to R^2 of the expert model. This is understandable in view of the similarity of local chemical environments for P and Ge atoms in these crystals (see Figure 2). In many promising SEs, they are present as $(XS_4)^{-q}$ polyanionic moieties with X = P, Ge, etc., in the sea of Li^+ ions and do not directly interact with each other. By combination of the ML models for the simpler crystals we can simulate the composite ones without any additional training. Therefore, the models trained in this study can be useful for modeling composite SEs, solutions, etc., which are widely applied for tailoring the performance of SEs. At last, since the computational cost of SGPR is proportional to the number of atoms N in the system, much bigger systems can be efficiently simulated compared with DFT where the computational cost scales as $\sim N^3$. This allows us to study the optimal composition with much higher resolution than accessible with AIMD.

In conclusion, we performed a survey of ternary crystals for fast Li-conducting electrolytes. $Li_{10}GeP_2S_{12}$ is also studied as a special quaternary case. Extensive MD simulations are carried out with on-the-fly ML of the potential energy using the SGPR algorithm. Most of the fastest ionic conductors found in this survey are already well-known electrolytes, which indicates the versatility of the applied methodology. We showed that models generated with kernel-based methods such as SGPR can be easily combined for more generality and transferability. Therefore, using the previously trained models in the database, it is possible to model new crystals without further training. This approach is demonstrated by creating universal potentials for two ternary systems. Additionally combinations of two ternary crystals resulted in an accurate potential for a quaternary crystal. With the introduced algorithm, the models generated in this study can be reused, with limited or no training at all, to describe more complex system (such as quaternary electrolytes) by a combinatorial approach.

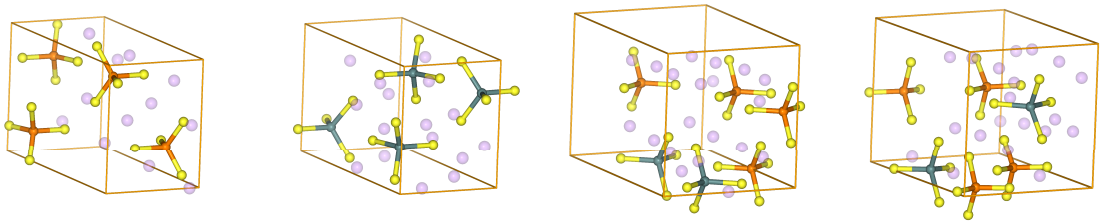

(a) Li_3PS_4 (b) Li_4GeS_4 (c) $Li_{10}GeP_2S_{12}$ (d) $Li_{10}GeP_2S_{12}$

Figure 2. In all of the above SEs, XS_4 polyanionic moieties are present with X = P or Ge.

https://doi.org/10.1021/acs.jpclett.1c01605
J. Phys. Chem. Lett. 2021, 12, 8115−8120

■ ASSOCIATED CONTENT

Supporting Information

The Supporting Information is available free of charge at https://pubs.acs.org/doi/10.1021/acs.jpclett.1c01605.

List of all considered ternary crystals and their selection criteria, ML details, MD details, MSDs of atoms during MD simulations for the fastest Li conductors, and statistical variances (PDF)

■ AUTHOR INFORMATION

Corresponding Author

Kwang S. Kim − *Center for Superfunctional Materials, Department of Chemistry and Department of Physics, Ulsan National Institute of Science and Technology, Ulsan 44919, Republic of Korea;* orcid.org/0000-0002-6929-5359; Email: kimks@unist.ac.kr

Author

Amir Hajibabaei − *Center for Superfunctional Materials, Department of Chemistry and Department of Physics, Ulsan National Institute of Science and Technology, Ulsan 44919, Republic of Korea;* orcid.org/0000-0003-1123-4040

Complete contact information is available at: https://pubs.acs.org/10.1021/acs.jpclett.1c01605

Notes

The authors declare no competing financial interest.

■ ACKNOWLEDGMENTS

This work was supported by the A.I. Incubation Project Fund (1.210091.01) of UNIST, NRF (National Honor Scientist Program: 2010-0020414), and KISTI (KSC-2018-CHA-0057, KSC-2019-CRE-0253, and KSC-2020-CRE-0146).

■ REFERENCES

(1) Deng, Z.; Mo, Y.; Ong, S. P. Computational Studies of Solid-State Alkali Conduction in Rechargeable Alkali-Ion Batteries. *NPG Asia Mater.* **2016**, *8*, e254.

(2) Famprikis, T.; Canepa, P.; Dawson, J. A.; Islam, M. S.; Masquelier, C. Fundamentals of Inorganic Solid-State Electrolytes for Batteries. *Nat. Mater.* **2019**, *18*, 1278−1291.

(3) Mo, Y.; Ong, S. P.; Ceder, G. First Principles Study of the $Li_{10}GeP_2S_{12}$ Lithium Super Ionic Conductor. *Chem. Mater.* **2012**, *24*, 15−17.

(4) Xu, M.; Ding, J.; Ma, E. One-dimensional Stringlike Cooperative Migration of Lithium Ions in an Ultrafast Ionic Conductor. *Appl. Phys. Lett.* **2012**, *101*, 031901.

(5) Chu, I. H.; Nguyen, H.; Hy, S.; Lin, Y. C.; Wang, Z.; Xu, Z.; Deng, Z.; Meng, Y. S.; Ong, S. P. Insights into the Performance Limits of the $Li_7P_3S_{11}$ Superionic Conductor: A Combined First-Principles and Experimental Study. *ACS Appl. Mater. Interfaces* **2016**, *8*, 7843−7853.

(6) Moon, J.; Lee, B.; Cho, M.; Cho, K. Ab Initio and Kinetic Monte Carlo Study of Lithium Diffusion in LiSi, $Li_{12}Si_7$, $Li_{13}Si_5$ and $Li_{15}Si_4$. *J. Power Sources* **2016**, *328*, 558−566.

(7) Ong, S. P.; Mo, Y.; Richards, W. D.; Miara, L.; Lee, H. S.; Ceder, G. Phase Stability, Electrochemical Stability and Ionic Conductivity of the $Li_{10\pm1}MP_2X_{12}$ (M = Ge, Si, Sn, Al or P, and X = O, S or Se) Family of Superionic Conductors. *Energy Environ. Sci.* **2013**, *6*, 148−156.

(8) Meier, K.; Laino, T.; Curioni, A. Solid-State Electrolytes: Revealing the Mechanisms of Li-Ion Conduction in Tetragonal and Cubic LLZO by First-Principles Calculations. *J. Phys. Chem. C* **2014**, *118*, 6668−6679.

(9) Jalem, R.; Yamamoto, Y.; Shiiba, H.; Nakayama, M.; Munakata, H.; Kasuga, T.; Kanamura, K. Concerted Migration Mechanism in the Li Ion Dynamics of Garnet-Type $Li_7La_3Zr_2O_{12}$. *Chem. Mater.* **2013**, *25*, 425−430.

(10) Deng, Z.; Radhakrishnan, B.; Ong, S. P. Rational Composition Optimization of the Lithium-Rich $Li_3OCl_{1-x}Br_x$ Anti-Perovskite Superionic Conductors. *Chem. Mater.* **2015**, *27*, 3749−3755.

(11) Deng, Y.; Eames, C.; Chotard, J.-N.; Lalère, F.; Seznec, V.; Emge, S.; Pecher, O.; Grey, C. P.; Masquelier, C.; Islam, M. S. Structural and Mechanistic Insights into Fast Lithium-Ion Conduction in Li_4SiO_4-Li_3PO_4 Solid Electrolytes. *J. Am. Chem. Soc.* **2015**, *137*, 9136−9145.

(12) He, X.; Zhu, Y.; Mo, Y. Origin of Fast Ion Diffusion In Super-Ionic Conductors. *Nat. Commun.* **2017**, *8*, 15893.

(13) He, X.; Zhu, Y.; Epstein, A.; Mo, Y. Statistical Variances of Diffusional Properties from Ab Initio Molecular Dynamics Simulations. *npj Comput. Mater.* **2018**, *4*, 18.

(14) Behler, J.; Parrinello, M. Generalized Neural-Network Representation of High-Dimensional Potential-Energy Surfaces. *Phys. Rev. Lett.* **2007**, *98*, 146401.

(15) Zhang, L.; Han, J.; Wang, H.; Car, R.; E, W. Deep Potential Molecular Dynamics: A Scalable Model with the Accuracy of Quantum Mechanics. *Phys. Rev. Lett.* **2018**, *120*, 143001.

(16) Schütt, K. T.; Gastegger, M.; Tkatchenko, A.; Müller, K. R.; Maurer, R. J. Unifying Machine Learning and Quantum Chemistry − a Deep Neural Network for Molecular Wavefunctions. *Nat. Commun.* **2019**, *10*, 5024.

(17) Bartók, A. P.; Payne, M. C.; Kondor, R.; Csányi, G. Gaussian Approximation Potentials: The Accuracy of Quantum Mechanics, without the Electrons. *Phys. Rev. Lett.* **2010**, *104*, 136403.

(18) Chmiela, S.; Tkatchenko, A.; Sauceda, H. E.; Poltavsky, I.; Schütt, K. T.; Müller, K.-R. Machine Learning of Accurate Energy-Conserving Molecular Force Fields. *Sci. Adv.* **2017**, *3*, e1603015.

(19) Chmiela, S.; Sauceda, H. E.; Müller, K.-R.; Tkatchenko, A. Towards Exact Molecular Dynamics Simulations With Machine-Learned Force Fields. *Nat. Commun.* **2018**, *9*, 3887.

(20) Seko, A.; Takahashi, A.; Tanaka, I. First-Principles Interatomic Potentials for Ten Elemental Metals via Compressed Sensing. *Phys. Rev. B: Condens. Matter Mater. Phys.* **2015**, *92*, 054113.

(21) Jinnouchi, R.; Karsai, F.; Kresse, G. On-the-Fly Machine Learning Force Field Generation: Application to Melting Points. *Phys. Rev. B: Condens. Matter Mater. Phys.* **2019**, *100*, 014105.

(22) Jinnouchi, R.; Lahnsteiner, J.; Karsai, F.; Kresse, G.; Bokdam, M. Phase Transitions of Hybrid Perovskites Simulated by Machine-Learning Force Fields Trained On the Fly with Bayesian Inference. *Phys. Rev. Lett.* **2019**, *122*, 225701.

(23) Hajibabaei, A.; Myung, C. W.; Kim, K. S. Sparse Gaussian Process Potentials: Application to Lithium Diffusivity in Superionic Conducting Solid Electrolytes. *Phys. Rev. B: Condens. Matter Mater. Phys.* **2021**, *103*, 214102.

(24) Li, Z.; Kermode, J. R.; De Vita, A. Molecular Dynamics with On-the-Fly Machine Learning of Quantum-Mechanical Forces. *Phys. Rev. Lett.* **2015**, *114*, 096405.

(25) Vandermause, J.; Torrisi, S. B.; Batzner, S.; Xie, Y.; Sun, L.; Kolpak, A. M.; Kozinsky, B. On-the-Fly Active Learning of Interpretable Bayesian Force Fields for Atomistic Rare Events. *npj Comput. Mater.* **2020**, *6*, 20.

(26) Prezhdo, O. V. Advancing Physical Chemistry with Machine Learning. *J. Phys. Chem. Lett.* **2020**, *11*, 9656.

(27) Deng, Z.; Chen, C.; Li, X. G.; Ong, S. P. An Electrostatic Spectral Neighbor Analysis Potential for Lithium Nitride. *npj Comput. Mater.* **2019**, *5*, 1−8.

(28) Li, W.; Ando, Y.; Minamitani, E.; Watanabe, S. Study of Li Atom Diffusion in Amorphous Li_3PO_4 With Neural Network Potential. *J. Chem. Phys.* **2017**, *147*, 214106.

(29) Bartók, A. P.; Kondor, R.; Csányi, G. On Representing Chemical Environments. *Phys. Rev. B: Condens. Matter Mater. Phys.* **2013**, *87*, 184115.

(30) Kresse, G.; Furthmüller, J. Efficient Iterative Schemes for Ab Initio Total-Energy Calculations Using a Plane-Wave Basis Set. *Phys. Rev. B: Condens. Matter Mater. Phys.* **1996**, *54*, 11169−11186.
(31) Blöchl, P. E. Projector Augmented-Wave Method. *Phys. Rev. B: Condens. Matter Mater. Phys.* **1994**, *50*, 17953−17979.
(32) Perdew, J. P.; Ernzerhof, M.; Burke, K. Rationale for Mixing Exact Exchange with Density Functional Approximations. *J. Chem. Phys.* **1996**, *105*, 9982−9985.
(33) Jain, A.; Ong, S. P.; Hautier, G.; Chen, W.; Richards, W. D.; Dacek, S.; Cholia, S.; Gunter, D.; Skinner, D.; Ceder, G.; et al. Commentary: The Materials Project: A Materials Genome Approach to Accelerating Materials Innovation. *APL Mater.* **2013**, *1*, 011002.
(34) Kamaya, N.; Homma, K.; Yamakawa, Y.; Hirayama, M.; Kanno, R.; Yonemura, M.; Kamiyama, T.; Kato, Y.; Hama, S.; Kawamoto, K.; et al. A Lithium Superionic Conductor. *Nat. Mater.* **2011**, *10*, 682−686.
(35) Wohlmuth, D.; Epp, V.; Wilkening, M. Fast Li Ion Dynamics in the Solid Electrolyte $Li_7P_3S_{11}$ as Probed by ^{6,7}Li NMR Spin-Lattice Relaxation. *ChemPhysChem* **2015**, *16*, 2582−2593.
(36) Lian, P.-J.; Zhao, B.-S.; Zhang, L.-Q.; Xu, N.; Wu, M.-T.; Gao, X.-P. Inorganic Sulfide Solid Electrolytes for All-Solid-State Lithium Secondary Batteries. *J. Mater. Chem. A* **2019**, *7*, 20540−20557.
(37) Li, X.; Liang, J.; Yang, X.; Adair, K. R.; Wang, C.; Zhao, F.; Sun, X. Progress and Perspectives on Halide Lithium Conductors for All-Solid-State Lithium Batteries. *Energy Environ. Sci.* **2020**, *13*, 1429−1461.
(38) Yamane, H.; Shibata, M.; Shimane, Y.; Junke, T.; Seino, Y.; Adams, S.; Minami, K.; Hayashi, A.; Tatsumisago, M. Crystal Structure of a Superionic Conductor, $Li_7P_3S_{11}$. *Solid State Ionics* **2007**, *178*, 1163−1167.
(39) Liu, Z.; Fu, W.; Payzant, E. A.; Yu, X.; Wu, Z.; Dudney, N. J.; Kiggans, J.; Hong, K.; Rondinone, A. J.; Liang, C. Anomalous High Ionic Conductivity of Nanoporous β-Li_3PS_4. *J. Am. Chem. Soc.* **2013**, *135*, 975−978.
(40) Ziolkowska, D. A.; Arnold, W.; Druffel, T.; Sunkara, M.; Wang, H. Rapid and Economic Synthesis of a Li_7PS_6 Solid Electrolyte from a Liquid Approach. *ACS Appl. Mater. Interfaces* **2019**, *11*, 6015.
(41) Seino, Y.; Ota, T.; Takada, K.; Hayashi, A.; Tatsumisago, M. A Sulphide Lithium Super Ion Conductor is Superior to Liquid Ion Conductors for Use in Rechargeable Batteries. *Energy Environ. Sci.* **2014**, *7*, 627−631.
(42) Yamada, K.; Kumano, K.; Okuda, T. Lithium Superionic Conductors Li_3InBr_6 and $LiInBr_4$ Studied by ^{7}Li, ^{115}In NMR. *Solid State Ionics* **2006**, *177*, 1691−1695.

https://doi.org/10.1021/acs.jpclett.1c01605
J. Phys. Chem. Lett. 2021, 12, 8115−8120